NANO LETTERS

pubs.acs.org/NanoLett Letter

Resonance-Enhanced Excitation of Interlayer Vibrations in Atomically Thin Black Phosphorus

Nannan Mao, Yuxuan Lin, Ya-Qing Bie, Tomás Palacios, Liangbo Liang, Riichiro Saito, Xi Ling, Jing Kong,* and William A. Tisdale*

Cite This: *Nano Lett.* 2021, 21, 4809−4815 Read Online

ACCESS | Metrics & More | Article Recommendations | Supporting Information

ABSTRACT: The strength of interlayer coupling critically affects the physical properties of 2D materials such as black phosphorus (BP), where the electronic structure depends sensitively on layer thickness. Rigid-layer vibrations reflect directly the interlayer coupling strength in 2D van der Waals solids, but measurement of these characteristic frequencies is made difficult by sample instability and small Raman scattering cross sections in atomically thin elemental crystals. Here, we overcome these challenges in BP by performing resonance-enhanced low-frequency Raman scattering under an argon-protective environment. Interlayer breathing modes for atomically thin BP were previously unobservable under conventional (nonresonant) excitation but became strongly enhanced when the excitation energy matched the sub-band electronic transitions of few-layer BP, down to bilayer thicknesses. The measured out-of-plane interlayer force constant was found to be 10.1×10^{19} N/m^3 in BP, which is comparable to graphene. Accurate characterization of the interlayer coupling strength lays the foundation for future exploration of BP twisted structures and heterostructures.

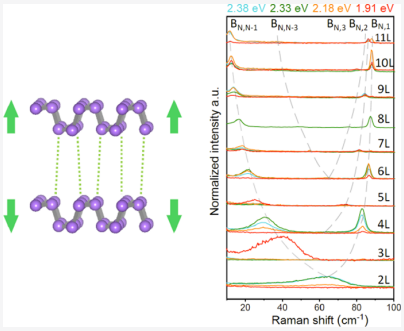

KEYWORDS: *rigid-layer lattice vibrations, black phosphorus, resonance Raman scattering, interlayer interaction, interband electronic transitions*

Interlayer interaction in two-dimensional (2D) materials plays a crucial role in electronic band structure evolution of atomically thin layered materials.[1,2] For example, MoS_2 undergoes a transition from indirect band gap in the bulk and few-layer to direct band gap in the monolayer, leading to significant excitonic character of the band edge absorption and emission spectra.[3] Moreover, 2D layers stacking together via van der Waals interaction with twisted angles have shown fascinating physical phenomena, such as superconductivity in magic angle graphene.[4] van der Waals interactions can also hold different combinations of 2D layers together, forming van der Waals heterostructures[5] that provide an exciting platform for the manipulation of interlayer excitons, electron−phonon, and electron−photon interactions.[6,7] Consequently, understanding the interlayer coupling in 2D materials is crucial for fundamental investigation of the physical properties of 2D materials and their heterostructured building blocks.

Black phosphorus (BP) is an emerging elemental 2D semiconductor, which has a puckered structure formed by sp^3 hybridized P atoms.[8−10] Due to the interlayer interaction, the valence band and conduction band in few-layer BP split into multiple sub-bands, giving rise to a thickness-dependent direct band gap and a series of optical resonances (called sub-band electronic transitions) between the van Hove singularities in the visible and infrared regime. Its band gap is tunable from 0.34 eV in the bulk to 1.73 eV in the atomically thin limit.[2,11] Given such sensitive dependence of the electronic structure on layer number, theoretical studies have explored the nature of interlayer interactions in BP, finding that these interactions arise in part from significant interlayer charge redistribution rather than pure van der Waals character.[12] Furthermore, the adhesion energy and the exfoliation energy in BP were predicted to be significantly larger than other 2D materials such as graphene and transition metal dichalcogenides (TMDs).[9,12−15] Therefore, understanding the interlayer interaction in BP is particularly important.

Collective interlayer vibrations in 2D materials, which usually occur at low frequency (<100 cm^{-1}), reflect directly the interlayer interaction between neighboring layers.[16−21] The effective interlayer force constant can be estimated either by (1) directly measuring the interlayer vibration frequency in bilayer samples or (2) fitting the layer-thickness-dependent frequency progression to a linear-chain model.[16,17,20,21] For

Received: April 8, 2021
Revised: May 19, 2021
Published: May 28, 2021

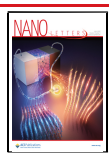

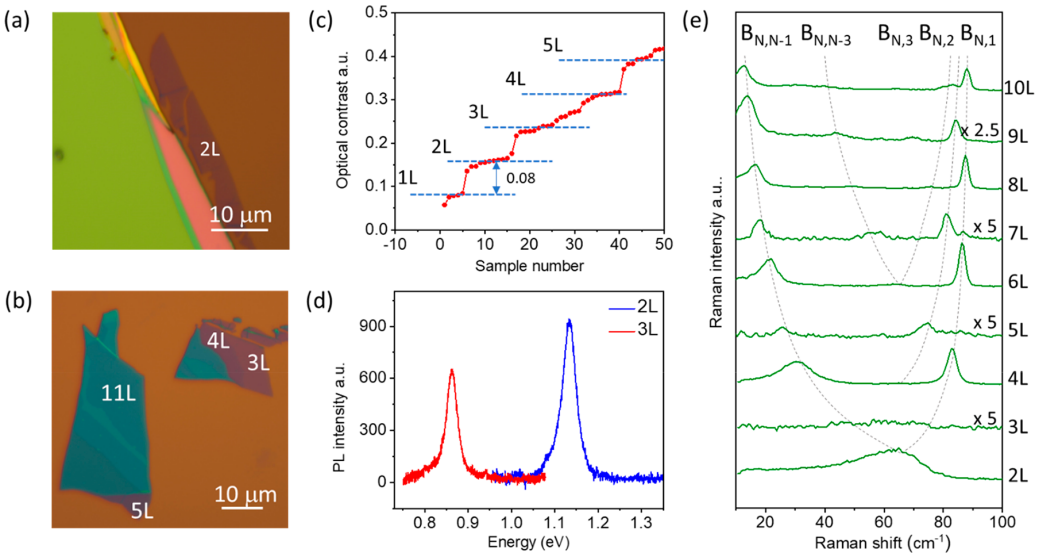

Figure 1. Characterization of few-layer phosphorus samples. (a,b) Optical images of few-layer BP samples marked with layer numbers. (c) Optical contrast (red channel) measured on 50 different few-layer BP samples; (d) photoluminescence spectra of 2L (blue line) and 3L (red line) BP samples excited at 635 nm. (e) Low-frequency Raman spectra of 2L−10L BP at the excitation energy of 2.33 eV. The Raman intensities of 3L, 5L, and 7L were scaled by 5 times and 9L by 2.5 times to illustrate high-order low-frequency Raman branches. The gray dash lines are guides for the eye.

BP, previous works have attempted to measure these collective interlayer oscillations under ambient conditions.[22−24] However, because the scattering probability of the interlayer vibrations in few-layer elemental 2D materials is extremely low,[16,25,26] assignment of the low-frequency Raman spectrum has proved challenging.[22−24] Moreover, the poor stability of few-layer BP samples under atmospheric conditions makes it difficult to determine their thicknesses precisely.[22−24] Such difficulties have led to inconsistent assignments of the lowest-frequency Raman-active mode in few-layer BP as either the interlayer breathing mode between BP layers[23,24] or the in-phase compression mode of the entire BP flake relative to the substrate.[22] These difficulties further make it challenging to accurately measure the interlayer coupling strength in BP.[22−24]

Here, we overcome the challenges of low-frequency Raman scattering in atomically thin BP by measuring resonance-enhanced Raman scattering under an argon-protective atmosphere. Interlayer vibration modes that were unobservable at conventional excitation wavelengths became strongly enhanced when the excitation energy matched an interband electronic transition above the band gap. We observe the full series of thickness-dependent interlayer vibrations in 2L−11L (L = layer) BP and show that the resonance effect is a critical consideration for the observation of the interlayer vibration modes in 2L and 3L BP. The lowest-energy mode shifts in frequency from 63.3 cm^{-1} for the bilayer to 11.8 cm^{-1} for 11L, consistent with a linear-chain model prediction of the variation of interlayer vibrational frequency with flake thickness. Using these experimentally measured frequencies, we find the out-of-plane interlayer force constant to be 10.1×10^{19} N/m^3 in BP, which is comparable to graphene (10.2×10^{19} N/m^3).[26] This work offers fundamental insights into the interlayer interaction in BP, which will facilitate the understanding and future exploration of the BP-related twisted structure and heterostructure.

RESULTS AND DISCUSSION

Few-layer BP samples (Figure 1a,b) were mechanically exfoliated onto a 285 nm SiO_2/Si substrate in an argon-gas glovebox. Their thicknesses were determined by optical contrast[27] and photoluminescence (PL) spectra measured under an inert argon atmosphere (see details in the Supporting Information). Optical contrasts of more than 50 few-layer BP samples were analyzed by extracting the pixel intensity value of the red channel from full-color optical images. They display a step-like increase with the thickness (Figures 1c and S1), suggesting linear dependence of optical contrast on BP thickness, with an optical contrast of around 0.08 for 1L BP. This calibration series allowed us to accurately determine the thickness of few-layer BP samples, as annotated in Figure 1a,b. The 2L and 3L BP were further confirmed to show PL peaks at 1.13 eV (1095 nm, Figure 1d) and 0.86 eV (1438 nm), respectively, which are consistent with previous reports.[2]

Figure 1e shows low-frequency Raman spectra in 2L−10L BP excited at 2.33 eV and measured under parallel polarization with both the incident and collection polarizations along the armchair (AC) direction of BP (Supporting Information). Crystalline orientations of these samples were identified by angle-dependent polarized Raman intensities of high-frequency Raman modes.[10,28−30] Notably, we were able to observe one broad low-frequency Raman peak at 63.3 cm^{-1} in 2L BP, which has not previously been reported. Moreover, five low-frequency Raman branches were observed in Figures 1e and S2, labeled as $B_{N,1}$, $B_{N,2}$, $B_{N,3}$, $B_{N,N-3}$, and $B_{N,N-1}$, where N is the layer number of the BP sample. Three of these branches blue-shift with increasing layer number, while two of them red-shift. The $B_{N,N-1}$ mode was observed for nearly all of the thicknesses (except 3L at 2.33 eV excitation), red-shifting as the thickness increases from 63.3 cm^{-1} in 2L BP to 12.7 cm^{-1} in 10 L BP. The highest-frequency branch, $B_{N,1}$, was consistently observed in even-layer BP samples, while the second-highest-frequency

https://doi.org/10.1021/acs.nanolett.1c00917
Nano Lett. 2021, 21, 4809−4815

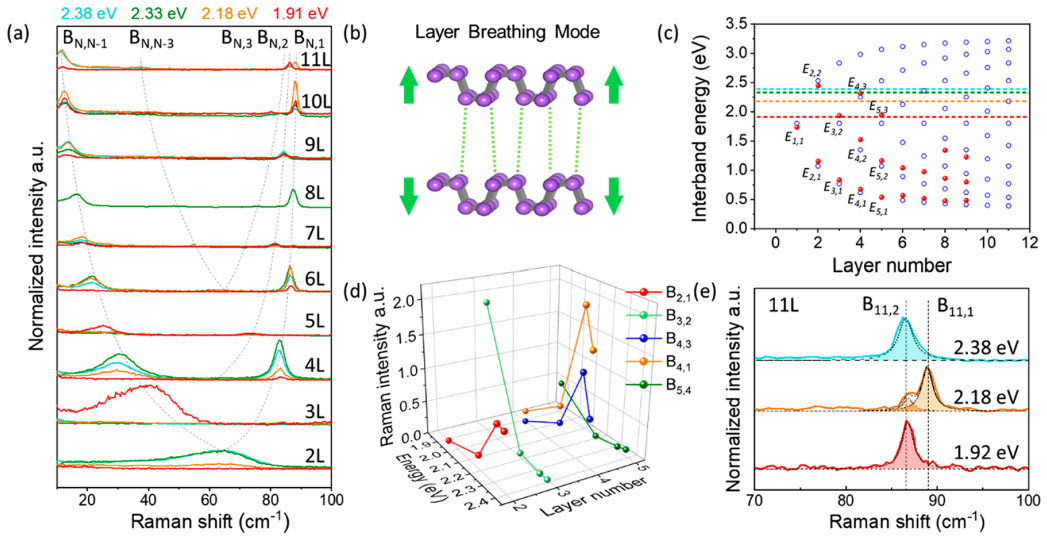

Figure 2. Resonance excitation of interlayer vibrations in few-layer BP. (a) Normalized low-frequency Raman spectra of 2L−11L BP excited at 2.38 (blue), 2.33 (green), 2.18 (orange), and 1.91 eV (red). The gray dash lines are guides for the eye to highlight the frequency shift of interlayer vibration modes. (b) Displacement pattern of the interlayer breathing mode in 2L BP. (c) Four Raman excitation energies (dashed lines) with respect to the calculated (blue opened circles) and measured (red dots) sub-band transition energies in few-layer BP from previous reports. Data reproduced from refs 2, 32, and 33. (d) Excitation-energy-dependent Raman intensities of the interlayer vibration modes in 2L−5L BP. (e) Normalized Raman spectra of 11L BP excited at 2.38, 2.18, and 1.91 eV. The black dash lines are guides for the eye to highlight the same interlayer vibration modes.

branch, $B_{N,2}$, was observed selectively in odd-layer BP samples. These trends are consistent with group theory analysis and first-principles calculations for interlayer breathing modes of BP in prior works,[14,22−24,31] confirming that all branches observed in Figure 1e are interlayer breathing modes.

Figure 2a displays low-frequency Raman spectra in 2L−11L BP excited at 2.38, 2.33, 2.18, and 1.91 eV, with both the incident and collection polarizations along the AC direction. They were normalized to the Raman intensity of a reference single crystalline quartz peak at 465 cm^{-1}. Raman frequencies at different excitation energies are calibrated by the silicon Raman peak at 520.7 cm^{-1} (Supporting Information, Table S1).

From the normalized Raman spectra under multiple excitation energies, we were able to observe low-frequency Raman peaks for each thickness. Particularly, a broad Raman peak at 63.3 cm^{-1} ($B_{2,1}$) was observed in 2L BP at excitation energies of 2.38 and 2.33 eV. It corresponds to the interlayer breathing mode as illustrated in Figure 2b. For 3L BP, a significant peak at 39.0 cm^{-1} was observed at 1.91 eV. The frequency difference of 2L and 3L BP is 24.3 cm^{-1}, which is comparable to that in graphene (24 cm^{-1}) while much larger than that in transition metal dichalcogenides such as MoS_2 (12 cm^{-1})[18] and $MoTe_2$ (9 cm^{-1}).[19] The lowest-frequency branch $B_{N,N-1}$ red-shifts from 63.3 cm^{-1} in 2L to 11.8 cm^{-1} for 11L BP, which matches well with the coherent phonon modes observed by transient absorption.[34]

The excitation energy dependence of the low-frequency Raman spectra in few-layer BP, as shown in Figure 2a, is a striking consequence of electronic resonance. For example, the breathing mode $B_{2,1}$ in 2L, which is hardly noticeable at an excitation energy of 1.91 eV, shows slightly stronger intensity at 2.18 eV and turns into a very broad and salient peak at 63.3 cm^{-1} when excited at 2.33 and 2.38 eV. In contrast, for 3L BP, a significant low-frequency Raman peak at 39.0 cm^{-1} appears at an excitation of 1.91 eV, while it is absent at other excitation energies. This phenomenon can be attributed to the intrinsic resonance effect with sub-band electronic transitions above the band gap. Due to quantum confinement and strong interlayer interaction, the conduction band and valence band of few-layer split into N quantized sub-bands $E_{N,n}$ at the Γ point of Brillouin zone (Figure S3), whose energies are in the visible and near-infrared region, where $E_{N,n}$ represents the n^{th} (n = 1, 2, 3, ..., N − 1) sub-band electronic transitions in NL BP (Figure 2c).[2,32,33] When the excitation energy matches with one of the sub-band electronic transitions, the Raman intensity of the corresponding breathing modes will be dramatically enhanced.[35−37]

For instance, as confirmed previously by the optical reflection measurement,[2] excitation lasers with energies of 2.38 (blue line) and 2.33 eV (green line) are in near resonance with the second sub-band electronic transition $E_{2,2}$ (2.44 eV) in 2L BP (Figure 2c). Consequently, it leads to strong low-frequency Raman intensities of 2L at 2.38 and 2.33 eV (Figure 2a,d). This also explains why the low-frequency Raman peak at 63.3 cm^{-1} was not observed in 2L BP in previous investigations where the excitation wavelength was limited to 633 nm (1.96 eV),[22−24] which is out of the resonance window. (Note that the low-frequency Raman spectrum assigned to 2L BP in a previous report[22] is actually the same as the Raman spectrum we assign here to 3L BP.) On the other hand, the 1.91 eV (648 nm) excitation is closely resonant with $E_{3,3}$ (1.93 eV, Figure 2c) in 3L BP, leading to a strong low-frequency Raman peak at 39.0 cm^{-1}. These observations reinforce the importance of resonance effects for accurate determination of breathing modes in few-layer BP.

Similarly, Raman resonance for both $B_{4,1}$ and $B_{4,3}$ modes occurs at 2.33 eV in 4L BP, close to the energy of the third sub-band electronic transition $E_{4,3}$ (2.31 eV, Figure 2c). The 5L BP indeed shows the strongest Raman intensity at 1.91 eV,

https://doi.org/10.1021/acs.nanolett.1c00917
Nano Lett. 2021, 21, 4809−4815

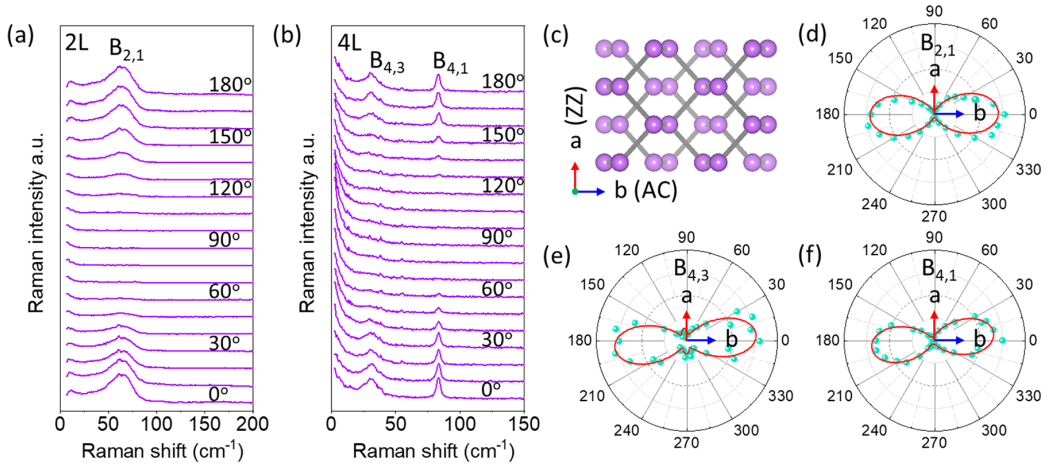

Figure 3. Symmetry assignment of interlayer vibrations in BP. (a,b) Polarization-dependent low-frequency Raman spectra of 2L and 4L BP excited at 2.33 and 2.18 eV, respectively. (c) The top view of the atomic structure of monolayer BP with *a* and *b* indicating zigzag (ZZ) and armchair (AC) crystalline orientations, respectively. (d–f) Polar plots of polarization-dependent Raman intensities of breathing modes $B_{2,1}$ (d) in 2L as well as $B_{4,3}$ (e) and $B_{4,1}$ (f) in 4L BP.

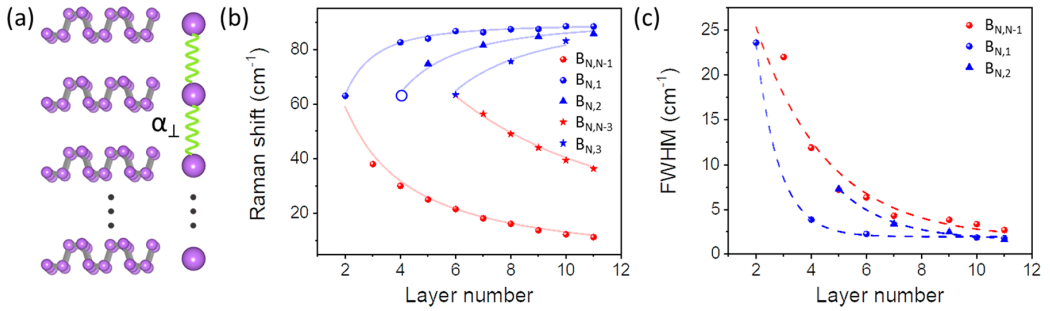

Figure 4. Frequency evolution of the interlayer breathing mode as explained by the linear-chain model. (a) Schematic illustration of the linear-chain model applied to BP. (b,c) Lorentzian-fitted frequency (b) and full width at half-maximum (fwhm) of the measured interlayer breathing mode as a function of thickness. Dashed lines are guides to the eye.

which matches the energy of the third sub-band electronic transition $E_{5,3}$ (1.94 eV, Figure 2c).

However, as the layer number further increases (and the electronic band gap continues to decrease), only high-order sub-bands ($E_{N,n}$, $n > 3$, Figure 2c) remain within the energy range of Raman excitation lines. For these thicker BP samples, optical interference effects can become dominant over resonance effects (Figure S4 and Table S2). The excitation energy that gives strongest Raman intensity might deviate from the interband transition energies. More discussions on multiple possible explanations for this discrepancy can be found in the Supporting Information.

In addition to enhancement of the Raman-active modes, resonance effects also contribute to the emergence of infrared-active modes in the Raman spectra.[38,39] According to the theoretical results,[31] the $B_{N,1}$ mode in odd-layer BP has B_{2u} symmetry, which is infrared-active rather than Raman-active. Under nonresonant conditions, for instance when the excitation energies are at 2.38 and 1.91 eV, this mode was not observed in the Raman spectra of 11L BP. However, when excited at 2.18 eV—which is resonant with $E_{11,7}$ (Figure 2c)—a bright peak at 88.1 cm^{-1} ($B_{11,1}$) appears in the Raman spectra (Figure 2e).

The assignment of the low-frequency modes in BP is vital to specify the type of interlayer interaction: in-plane shear or out-of-plane compression. To further verify the symmetry assignment of the observed interlayer vibrational modes, we measured the polarization-dependent low-frequency Raman spectra of 2L and 4L BP. As shown in Figure 3a,b, Raman spectra of both samples vary significantly with the sample rotation angle under parallel polarization. All of the low-frequency Raman peaks show the largest intensity with the laser polarized along the AC (0°) direction, while they almost disappear along the ZZ direction (90°). Crystalline orientations of BP are illustrated in Figure 3c. The intensity polar plots of $B_{2,1}$, $B_{4,3}$, and $B_{4,1}$ show a local maximum and minimum when both incident and collection polarizations are along the crystalline orientations of BP (Figure 3d–f), suggesting that all of them are indeed interlayer breathing modes of A_g symmetry.[23,28−30,40−42]

The Raman spectra of $B_{N,N-1}$ modes in 2L and 3L BP are asymmetrically broadened toward the low-energy side, as shown in Figure S5. Asymmetric line shapes of low-frequency Raman modes have been observed in graphene,[16] Bi_2Se_3,[43] and 2D semiconductors such as WS_2.[39] In those systems, the asymmetry was attributed to Fano resonances, i.e., quantum interference between a discrete phonon state and a continuum

https://doi.org/10.1021/acs.nanolett.1c00917
Nano Lett. 2021, 21, 4809−4815

of electronic transitions.[16,39,43] We find that the asymmetric modes in 2L and 3L BP can be fit well by a Fano line shape (Table S3), but the origin of the Fano resonance—and its strong dependence on flake thickness—is unclear. See Supporting Information for a complete discussion.

The layer-number-dependent frequency of interlayer breathing modes can be well-described by the linear-chain model,[16,17,20,21] which treats each layer as a rigid "ball" connected to its neighboring layers by a classical spring. Considering only nearest-neighbor interactions (Figure 4a), this model gives rise to N-dependent frequencies

$$\omega(B_{N,N-j}) = \sqrt{2}\,\omega(B_{2,1})\sin\left(\frac{j\pi}{2N}\right) \quad (1)$$

where $\omega(B_{2,1})$ is the frequency of the breathing mode in 2L BP, and j = 1, 2, ..., N − 1 is the branch index. As shown in Figure 4b, all branches can be fitted well by the linear-chain model. As listed in Table S4, the fitted $\omega(B_{2,1})$ values are very close to the measured frequency of the breathing mode in 2L BP. Our analysis confirms that all of the observed branches—including the $B_{N,N-1}$ mode—are interlayer breathing modes,[23,24] which are in-phase or out-of-phase vibrations of BP layers relative to neighboring BP layers in the out-of-plane direction. Particularly, we clarify that the $B_{N,N-1}$ branch is interlayer vibrations in BP rather than a collective compression mode of the entire BP stack relative to the substrate.[22]

Based on our measured breathing mode frequency of $\omega(B_{2,1})$ = 63.3 cm^{-1} in 2L BP and the relation from the linear-chain model $\omega(B_{bulk}) = \sqrt{2}\,\omega(B_{2,1})$, we can derive $\omega(B_{bulk})$ to be 89.5 cm^{-1} for bulk BP, consistent with the experimental value of ∼87 cm^{-1} from inelastic neutron scattering measurements.[44,45] The full width at half-maximum (fwhm) of the interlayer breathing mode broadens as the thickness decreases (Figure 4c). This trend may arise from easier dissipation of phonon energy into the surrounding environment for thinner flakes.

The strength of the out-of-plane interaction in bilayer BP can be estimated by[16,17]

$$\omega(B_{2,1}) = 1/(\sqrt{2}\pi c)\sqrt{\alpha/\mu} \quad (2)$$

where c is the speed of light and μ = 1.42 × 10^{-26} kg Å^{-2} is the mass per unit cell area in BP. Using eq 2 and the measured frequency in bilayer BP of 63.3 cm^{-1}, the out-of-plane interlayer force constant is found to be α = 10.1 × 10^{19} N/m^3. This value is close to the interlayer force constant reported for other 2D vdW materials (α is 10.2 × 10^{19} and 8.9 × 10^{19} N/m^3 for graphene[25,46] and MoS_2,[18] respectively). The similarity between the interlayer force constant in BP and in other 2D vdW materials is surprising given previous estimates that interlayer interactions are stronger in BP than in graphene and MoS_2.[22,24] One study noted that since BP has a highly corrugated structure, where only half of the atoms per unit area are involved in nearest-neighbor interactions, it might be fairer to compare interlayer force constants on a per-atom basis.[14] In this scenario, the renormalized out-of-plane constant is 7.3 N/atom in BP, which is 2.8 times stronger than in graphene (2.6 N/atom).

In summary, we measured the interlayer coupling strength of BP using resonance low-frequency Raman spectra under an argon-gas environment and found the interlayer coupling constant to be 10.1 × 10^{19} N/m^3, which is comparable to that of graphene. Accurate determination of the interlayer force constant was made possible by careful calibration of the layer thickness and resonance enhancement of the Raman intensity through variation of the excitation laser energy relative to interband electronic transitions in few-layer BP. The interlayer vibrational modes in atomically thin elemental 2D materials, which are generally too weak to be observed especially in 2L–3L BP, show significant Raman enhancement under resonance excitation. All of the interlayer vibration modes observed in our experiment are confirmed to be interlayer breathing modes in few-layer BP, which show thickness-dependent frequency and resonance effects in agreement with the linear-chain model. The accurate identification of these frequencies also provides a quick and reliable way to determine the thickness of few-layer BP samples. The strong interlayer coupling of BP offers promising possibilities to design and construct new optoelectronic devices based on the twisted structure and heterostructure related to BP.

■ ASSOCIATED CONTENT

Supporting Information

The Supporting Information is available free of charge at https://pubs.acs.org/doi/10.1021/acs.nanolett.1c00917.

Methods; thickness determination; low-frequency Raman modes in few-layer BP; resonance and interference enhancement in thicker layer; Fano line analysis of asymmetric modes; Figures S1–S5; Tables S1–S4 (PDF)

■ AUTHOR INFORMATION

Corresponding Authors

Jing Kong − *Department of Electrical Engineering and Computer Science, Massachusetts Institute of Technology, Cambridge, Massachusetts 02139, United States;* orcid.org/0000-0003-0551-1208; Email: jingkong@mit.edu

William A. Tisdale − *Department of Chemical Engineering, Massachusetts Institute of Technology, Cambridge, Massachusetts 02139, United States;* orcid.org/0000-0002-6615-5342; Email: tisdale@mit.edu

Authors

Nannan Mao − *Department of Electrical Engineering and Computer Science and Department of Chemical Engineering, Massachusetts Institute of Technology, Cambridge, Massachusetts 02139, United States; Department of Chemistry and Division of Materials Science and Engineering, Boston University, Boston, Massachusetts 02215, United States;* orcid.org/0000-0003-3522-5341

Yuxuan Lin − *Department of Electrical Engineering and Computer Science, Massachusetts Institute of Technology, Cambridge, Massachusetts 02139, United States*

Ya-Qing Bie − *Department of Physics, Massachusetts Institute of Technology, Cambridge, Massachusetts 02139, United States;* orcid.org/0000-0003-2755-9472

Tomás Palacios − *Department of Electrical Engineering and Computer Science, Massachusetts Institute of Technology, Cambridge, Massachusetts 02139, United States;* orcid.org/0000-0002-2190-563X

Liangbo Liang − *Center for Nanophase Materials Sciences, Oak Ridge National Laboratory, Oak Ridge, Tennessee 37831, United States;* orcid.org/0000-0003-1199-0049

https://doi.org/10.1021/acs.nanolett.1c00917
Nano Lett. 2021, 21, 4809−4815

Riichiro Saito − *Department of Physics, Tohoku University, Sendai 980-8578, Japan*

Xi Ling − *Department of Chemistry and Division of Materials Science and Engineering and The Photonics Center, Boston University, Boston, Massachusetts 02215, United States;* orcid.org/0000-0003-3462-9088

Complete contact information is available at: https://pubs.acs.org/10.1021/acs.nanolett.1c00917

Author Contributions

N.M., J.K., W.A.T., X.L., and L.L. initiated the project and designed the experiments. N.M. and Y.-Q.B. prepared samples. N.M. and Y.L. performed the experimental measurements. N.M., W.A.T., J. K., X.L., R.S., and L.L. analyzed the data. All authors contributed to the writing of the paper.

Notes

The authors declare no competing financial interest.

■ ACKNOWLEDGMENTS

This work is primarily supported by the U.S. Department of Energy (DOE), Office of Science, Basic Energy Sciences (BES) under Award DE-SC0020042. J.K. and N.M. also acknowledge the partial support by the Air Force Office of Scientific Research under the MURI-FATE program, Grant No. FA9550-15-1-0514. W.A.T. acknowledges support from the Camille & Henry Dreyfus Foundation. Y.L., T.P., and J.K. also acknowledge the partial support by the U.S. Army Research Office through the Institute for Soldier Nanotechnologies at MIT, under cooperative agreement number W911NF-18-2-0048. X.L. acknowledges the support of National Science Foundation (NSF) under Grant No. (1945364). R.S. acknowledges JSPS KAKENHI (Grant No. JP18H01810). L.L. acknowledges work conducted at the Center for Nanophase Materials Sciences, which is a US Department of Energy Office of Science User Facility. The authors thank Q.M. and P.J.H. at MIT for assistance on PL measurement, sample preparation, and protection.

■ REFERENCES

(1) Novoselov, K. S.; Geim, A. K.; Morozov, S. V.; Jiang, D.; Zhang, Y.; Dubonos, S. V.; Grigorieva, I. V.; Firsov, A. A. Electric Field Effect in Atomically Thin Carbon Films. *Science* **2004**, *306*, 666−669.

(2) Li, L.; Kim, J.; Jin, C.; Ye, G. J.; Qiu, D. Y.; da Jornada, F. H.; Shi, Z.; Chen, L.; Zhang, Z.; Yang, F.; Watanabe, K.; Taniguchi, T.; Ren, W.; Louie, S. G.; Chen, X. H.; Zhang, Y.; Wang, F. Direct Observation of the Layer-Dependent Electronic Structure in Phosphorene. *Nat. Nanotechnol.* **2017**, *12*, 21−25.

(3) Splendiani, A.; Sun, L.; Zhang, Y.; Li, T.; Kim, J.; Chim, C.-Y.; Galli, G.; Wang, F. Emerging Photoluminescence in Monolayer MoS_2. *Nano Lett.* **2010**, *10*, 1271−1275.

(4) Cao, Y.; Fatemi, V.; Fang, S.; Watanabe, K.; Taniguchi, T.; Kaxiras, E.; Jarillo-Herrero, P. Unconventional Superconductivity in Magic-Angle Graphene Superlattices. *Nature* **2018**, *556*, 43−50.

(5) Geim, A. K.; Grigorieva, I. V. Van Der Waals Heterostructures. *Nature* **2013**, *499*, 419−425.

(6) Eliel, G. S. N.; Moutinho, M. V. O.; Gadelha, A. C.; Righi, A.; Campos, L. C.; Ribeiro, H. B.; Chiu, P.-W.; Watanabe, K.; Taniguchi, T.; Puech, P.; Paillet, M.; Michel, T.; Venezuela, P.; Pimenta, M. A. Intralayer and Interlayer Electron-Phonon Interactions in Twisted Graphene Heterostructures. *Nat. Commun.* **2018**, *9*, 1221.

(7) Rivera, P.; Schaibley, J. R.; Jones, A. M.; Ross, J. S.; Wu, S.; Aivazian, G.; Klement, P.; Seyler, K.; Clark, G.; Ghimire, N. J.; Yan, J.; Mandrus, D. G.; Yao, W.; Xu, X. Observation of Long-Lived Interlayer Excitons in Monolayer $Mose_2$-Wse_2 Heterostructures. *Nat. Commun.* **2015**, *6*, 6242.

(8) Li, L.; Yu, Y.; Ye, G. J.; Ge, Q.; Ou, X.; Wu, H.; Feng, D.; Chen, X. H.; Zhang, Y. Black Phosphorus Field-Effect Transistors. *Nat. Nanotechnol.* **2014**, *9*, 372−377.

(9) Qiao, J.; Kong, X.; Hu, Z.-X.; Yang, F.; Ji, W. High-Mobility Transport Anisotropy and Linear Dichroism in Few-Layer Black Phosphorus. *Nat. Commun.* **2014**, *5*, 4475.

(10) Xia, F.; Wang, H.; Jia, Y. Rediscovering Black Phosphorus as an Anisotropic Layered Material for Optoelectronics and Electronics. *Nat. Commun.* **2014**, *5*, 4458.

(11) Low, T.; Rodin, A. S.; Carvalho, A.; Jiang, Y.; Wang, H.; Xia, F.; Castro Neto, A. H. Tunable Optical Properties of Multilayer Black Phosphorus Thin Films. *Phys. Rev. B: Condens. Matter Mater. Phys.* **2014**, *90*, 075434.

(12) Shulenburger, L.; Baczewski, A. D.; Zhu, Z.; Guan, J.; Tománek, D. The Nature of the Interlayer Interaction in Bulk and Few-Layer Phosphorus. *Nano Lett.* **2015**, *15*, 8170−8175.

(13) Sansone, G.; Maschio, L.; Usvyat, D.; Schütz, M.; Karttunen, A. Toward an Accurate Estimate of the Exfoliation Energy of Black Phosphorus: A Periodic Quantum Chemical Approach. *J. Phys. Chem. Lett.* **2016**, *7*, 131−136.

(14) Hu, Z.-X.; Kong, X.; Qiao, J.; Normand, B.; Ji, W. Interlayer Electronic Hybridization Leads to Exceptional Thickness-Dependent Vibrational Properties in Few-Layer Black Phosphorus. *Nanoscale* **2016**, *8*, 2740−2750.

(15) Schütz, M.; Maschio, L.; Karttunen, A. J.; Usvyat, D. Exfoliation Energy of Black Phosphorus Revisited: A Coupled Cluster Benchmark. *J. Phys. Chem. Lett.* **2017**, *8*, 1290−1294.

(16) Tan, P. H.; Han, W. P.; Zhao, W. J.; Wu, Z. H.; Chang, K.; Wang, H.; Wang, Y. F.; Bonini, N.; Marzari, N.; Pugno, N.; Savini, G.; Lombardo, A.; Ferrari, A. C. The Shear Mode of Multilayer Graphene. *Nat. Mater.* **2012**, *11*, 294−300.

(17) Liang, L.; Zhang, J.; Sumpter, B. G.; Tan, Q.-H.; Tan, P.-H.; Meunier, V. Low-Frequency Shear and Layer-Breathing Modes in Raman Scattering of Two-Dimensional Materials. *ACS Nano* **2017**, *11*, 11777−11802.

(18) Zhang, X.; Han, W. P.; Wu, J. B.; Milana, S.; Lu, Y.; Li, Q. Q.; Ferrari, A. C.; Tan, P. H. Raman Spectroscopy of Shear and Layer Breathing Modes in Multilayer Mos_2. *Phys. Rev. B: Condens. Matter Mater. Phys.* **2013**, *87*, 115413.

(19) Froehlicher, G.; Lorchat, E.; Fernique, F.; Joshi, C.; Molina-Sánchez, A.; Wirtz, L.; Berciaud, S. Unified Description of the Optical Phonon Modes in N-Layer $Mote_2$. *Nano Lett.* **2015**, *15*, 6481−6489.

(20) Zhao, Y.; Luo, X.; Li, H.; Zhang, J.; Araujo, P. T.; Gan, C. K.; Wu, J.; Zhang, H.; Quek, S. Y.; Dresselhaus, M. S.; Xiong, Q. Interlayer Breathing and Shear Modes in Few-Trilayer Mos2 and Wse2. *Nano Lett.* **2013**, *13*, 1007−1015.

(21) He, R.; Yan, J.-A.; Yin, Z.; Ye, Z.; Ye, G.; Cheng, J.; Li, J.; Lui, C. H. Coupling and Stacking Order of Res2 Atomic Layers Revealed by Ultralow-Frequency Raman Spectroscopy. *Nano Lett.* **2016**, *16*, 1404−1409.

(22) Dong, S.; Zhang, A.; Liu, K.; Ji, J.; Ye, Y. G.; Luo, X. G.; Chen, X. H.; Ma, X.; Jie, Y.; Chen, C.; Wang, X.; Zhang, Q. Ultralow-Frequency Collective Compression Mode and Strong Interlayer Coupling in Multilayer Black Phosphorus. *Phys. Rev. Lett.* **2016**, *116*, 087401.

(23) Ling, X.; Liang, L.; Huang, S.; Puretzky, A. A.; Geohegan, D. B.; Sumpter, B. G.; Kong, J.; Meunier, V.; Dresselhaus, M. S. Low-Frequency Interlayer Breathing Modes in Few-Layer Black Phosphorus. *Nano Lett.* **2015**, *15*, 4080−4088.

(24) Luo, X.; Lu, X.; Koon, G. K. W.; Castro Neto, A. H.; Özyilmaz, B.; Xiong, Q.; Quek, S. Y. Large Frequency Change with Thickness in Interlayer Breathing Mode—Significant Interlayer Interactions in Few Layer Black Phosphorus. *Nano Lett.* **2015**, *15*, 3931−3938.

(25) Lui, C. H.; Heinz, T. F. Measurement of Layer Breathing Mode Vibrations in Few-Layer Graphene. *Phys. Rev. B: Condens. Matter Mater. Phys.* **2013**, *87*, 121404.

(26) Lui, C. H.; Malard, L. M.; Kim, S.; Lantz, G.; Laverge, F. E.; Saito, R.; Heinz, T. F. Observation of Layer-Breathing Mode Vibrations in Few-Layer Graphene through Combination Raman Scattering. *Nano Lett.* **2012**, *12*, 5539−5544.
(27) Ni, Z. H.; Wang, H. M.; Kasim, J.; Fan, H. M.; Yu, T.; Wu, Y. H.; Feng, Y. P.; Shen, Z. X. Graphene Thickness Determination Using Reflection and Contrast Spectroscopy. *Nano Lett.* **2007**, *7*, 2758−2763.
(28) Mao, N.; Wang, X.; Lin, Y.; Sumpter, B. G.; Ji, Q.; Palacios, T.; Huang, S.; Meunier, V.; Dresselhaus, M. S.; Tisdale, W. A.; Liang, L.; Ling, X.; Kong, J. Direct Observation of Symmetry-Dependent Electron-Phonon Coupling in Black Phosphorus. *J. Am. Chem. Soc.* **2019**, *141*, 18994−19001.
(29) Ling, X.; Huang, S.; Hasdeo, E. H.; Liang, L.; Parkin, W. M.; Tatsumi, Y.; Nugraha, A. R.; Puretzky, A. A.; Das, P. M.; Sumpter, B. G.; Geohegan, D. B.; Kong, J.; Saito, R.; Drndic, M.; Meunier, V.; Dresselhaus, M. S. Anisotropic Electron-Photon and Electron-Phonon Interactions in Black Phosphorus. *Nano Lett.* **2016**, *16*, 2260−2267.
(30) Wu, J.; Mao, N.; Xie, L.; Xu, H.; Zhang, J. Identifying the Crystalline Orientation of Black Phosphorus Using Angle-Resolved Polarized Raman Spectroscopy. *Angew. Chem., Int. Ed.* **2015**, *54*, 2366−2369.
(31) Cai, Y.; Ke, Q.; Zhang, G.; Feng, Y. P.; Shenoy, V. B.; Zhang, Y.-W. Giant Phononic Anisotropy and Unusual Anharmonicity of Phosphorene: Interlayer Coupling and Strain Engineering. *Adv. Funct. Mater.* **2015**, *25*, 2230−2236.
(32) Zhang, G.; Huang, S.; Chaves, A.; Song, C.; Özçelik, V. O.; Low, T.; Yan, H. Infrared Fingerprints of Few-Layer Black Phosphorus. *Nat. Commun.* **2017**, *8*, 14071.
(33) Zhang, G.; Chaves, A.; Huang, S.; Wang, F.; Xing, Q.; Low, T.; Yan, H. Determination of Layer-Dependent Exciton Binding Energies in Few-Layer Black Phosphorus. *Sci. Adv.* **2018**, *4*, No. eaap9977.
(34) Miao, X.; Zhang, G.; Wang, F.; Yan, H.; Ji, M. Layer-Dependent Ultrafast Carrier and Coherent Phonon Dynamics in Black Phosphorus. *Nano Lett.* **2018**, *18*, 3053−3059.
(35) McDonnell, L. P.; Huang, C. C.; Cui, Q.; Hewak, D. W.; Smith, D. C. Probing Excitons, Trions, and Dark Excitons in Monolayer Ws_2 Using Resonance Raman Spectroscopy. *Nano Lett.* **2018**, *18*, 1428−1434.
(36) Wu, J.-B.; Zhang, X.; Ijäs, M.; Han, W.-P.; Qiao, X.-F.; Li, X.-L.; Jiang, D.-S.; Ferrari, A. C.; Tan, P.-H. Resonant Raman Spectroscopy of Twisted Multilayer Graphene. *Nat. Commun.* **2014**, *5*, 5309.
(37) Cheong, H.; Lee, J.-U. Resonant Raman Spectroscopy of Two Dimensional Materials Beyond Graphene. *Springer Ser. Mater. Sci.* **2019**, *276*, 185−202.
(38) Tan, Q.-H.; Sun, Y.-J.; Liu, X.-L.; Xu, K.-X.; Gao, Y.-F.; Ren, S.-L.; Tan, P.-H.; Zhang, J. Breakdown of Raman Selection Rules by Fröhlich Interaction in Few-Layer Ws 2. *Nano Res.* **2021**, *14*, 239−244.
(39) Tan, Q.-H.; Sun, Y.-J.; Liu, X.-L.; Zhao, Y.; Xiong, Q.; Tan, P.-H.; Zhang, J. Observation of Forbidden Phonons, Fano Resonance and Dark Excitons by Resonance Raman Scattering in Few-Layer Ws 2. *2D Mater.* **2017**, *4*, 031007.
(40) Kim, J.; Lee, J. U.; Lee, J.; Park, H. J.; Lee, Z.; Lee, C.; Cheong, H. Anomalous Polarization Dependence of Raman Scattering and Crystallographic Orientation of Black Phosphorus. *Nanoscale* **2015**, *7*, 18708−18715.
(41) Phaneuf-L'Heureux, A. L.; Favron, A.; Germain, J. F.; Lavoie, P.; Desjardins, P.; Leonelli, R.; Martel, R.; Francoeur, S. Polarization-Resolved Raman Study of Bulk-Like and Davydov-Induced Vibrational Modes of Exfoliated Black Phosphorus. *Nano Lett.* **2016**, *16*, 7761−7767.
(42) Mao, N.; Zhang, S.; Wu, J.; Zhang, J.; Tong, L. Lattice Vibration and Raman Scattering in Anisotropic Black Phosphorus Crystals. *Small Methods* **2018**, *2*, 1700409.
(43) Zhang, J.; Peng, Z.; Soni, A.; Zhao, Y.; Xiong, Y.; Peng, B.; Wang, J.; Dresselhaus, M. S.; Xiong, Q. Raman Spectroscopy of Few-Quintuple Layer Topological Insulator Bi2se3 Nanoplatelets. *Nano Lett.* **2011**, *11*, 2407−2414.
(44) Fujii, Y.; Akahama, Y.; Endo, S.; Narita, S.; Yamada, Y.; Shirane, G. Inelastic Neutron Scattering Study of Acoustic Phonons of Black Phosphorus. *Solid State Commun.* **1982**, *44*, 579−582.
(45) Yamada, Y.; Fujii, Y.; Akahama, Y.; Endo, S.; Narita, S.; Axe, J. D.; McWhan, D. B. Lattice-Dynamical Properties of Black Phosphorus under Pressure Studied by Inelastic Neutron Scattering. *Phys. Rev. B: Condens. Matter Mater. Phys.* **1984**, *30*, 2410−2413.
(46) Lui, C. H.; Ye, Z.; Keiser, C.; Xiao, X.; He, R. Temperature-Activated Layer-Breathing Vibrations in Few-Layer Graphene. *Nano Lett.* **2014**, *14*, 4615−4621.

https://doi.org/10.1021/acs.nanolett.1c00917
Nano Lett. 2021, 21, 4809−4815